LANGMUIR Article
Cite This: Langmuir 2018, 34, 13745−13753
pubs.acs.org/Langmuir

Characterizing How Acidic pH Conditions Affect the Membrane-Disruptive Activities of Lauric Acid and Glycerol Monolaurate

Elba R. Valle-González,[†,‡] Joshua A. Jackman,[†,‡] Bo Kyeong Yoon,[†,‡] Soohyun Park,[†,‡] Tun Naw Sut,[†,‡] and Nam-Joon Cho*[,†,‡,§]

[†]School of Materials Science and Engineering, Nanyang Technological University, 50 Nanyang Avenue, 639798, Singapore
[‡]Centre for Biomimetic Sensor Science, Nanyang Technological University, 50 Nanyang Drive, 637553, Singapore
[§]School of Chemical and Biomedical Engineering, Nanyang Technological University, 62 Nanyang Drive, 637459, Singapore

Supporting Information

ABSTRACT: Fatty acids and monoglycerides are single-chain lipid amphiphiles that interact with phospholipid membranes as part of various biological activities. For example, they can exhibit membrane-disruptive behavior against microbial pathogens on the human skin surface. Supported lipid bilayers (SLBs) provide a useful experimental platform to characterize these membrane-disruptive behaviors, although related studies have been limited to neutral pH conditions. Herein, we investigated how lauric acid (LA) and glycerol monolaurate (GML) interact with SLBs and cause membrane morphological changes under acidic pH conditions that are representative of the human skin surface. Although LA induces tubule formation under neutral pH conditions, we discovered that LA causes membrane phase separation under acidic pH conditions. By contrast, GML induced membrane budding in both pH environments, although there was more extensive membrane remodeling under acidic pH conditions. We discuss these findings in the context of how solution pH affects the ionization states and micellar aggregation properties of LA and GML as well as its effect on the bending stiffness of lipid bilayers. Collectively, the findings demonstrate that solution pH plays an important role in modulating the interaction of fatty acids and monoglycerides with phospholipid membranes, and hence influences the scope and potency of their membrane-disruptive activities.

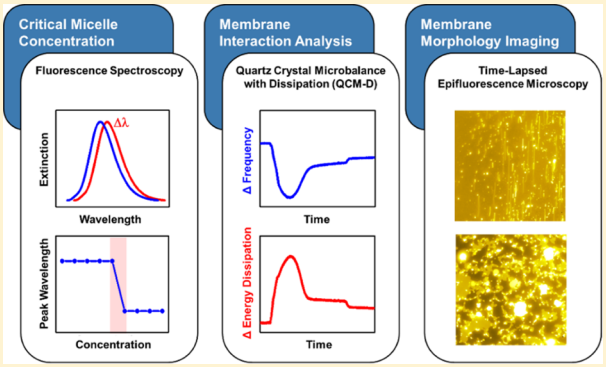

INTRODUCTION

The self-assembly of lipid molecules plays an important role in driving membrane organization[1,2] and facilitating biomedical applications such as drug delivery[3] and antimicrobial medicine.[4] Among the different types of lipids, fatty acids, and monoglycerides are single-chain lipid amphiphiles that exhibit broad-spectrum antimicrobial activity[5,6] and destabilize the cellular membranes of microbial pathogens.[7,8] Often referred to as "antimicrobial lipids", they are an integral part of the innate immune system on the human skin surface where their main function is to inhibit pathogens and regulate microbial populations.[9−11] Within this scope, it is known that medium-chain saturated fatty acids and monoglyceride derivatives have particularly high antibacterial activities.[12] Lauric acid (LA; C12:0) is regarded as the most inhibitory saturated fatty acid against Gram-positive bacteria.[13] Its monoglyceride derivative, glycerol monolaurate (GML), also has potent antibacterial effects; GML demonstrates greater potency (lower effective concentration), albeit against a narrower spectrum of susceptible bacteria.[13−16] These inhibitory effects have motivated experimental efforts to characterize how antimicrobial lipids destabilize cellular membrane targets.

Conventionally, the effects of antimicrobial lipids on cellular membranes have been assessed posttreatment by electron microscopy (EM) techniques, which enable visualization of membrane morphological changes and intracellular damage.[17,18] However, real-time monitoring of membrane interactions is not possible with EM, and similar challenges also exist for atomic force microscopy approaches.[19] To address these shortcomings, membrane fluidity and ion leakage assays have been conducted on bacterial cells posttreatment[20] along with transcriptomic-level analysis to characterize cellular responses.[21] Such approaches have enabled a deeper understanding of how membrane properties and cellular functions are affected by antimicrobial lipids. Complementing these approaches, there is significant opportunity to characterize the real-time interactions between antimicrobial lipids and phospholipid membranes by employing model systems in

Received: July 26, 2018
Revised: October 14, 2018
Published: October 20, 2018

DOI: 10.1021/acs.langmuir.8b02536
Langmuir 2018, 34, 13745−13753

conjunction with highly sensitive measurement techniques. Among the options, supported lipid bilayers (SLBs) provide a versatile, two-dimensional model membrane platform that is compatible with a variety of surface-sensitive measurement techniques.[22]

Yoon et al. utilized SLB platforms to distinguish the membrane morphological changes caused by fatty acids and monoglycerides.[14] It was shown that anionic LA induced the formation of elongated tubule structures, whereas nonionic GML caused membrane budding. The distinct membrane morphological responses were attributed to differences in the membrane translocation properties of anionic versus nonionic compounds,[23] and corresponding effects on membrane strain.[24] Importantly, the membrane-disruptive activities of LA and GML occurred at or above their respective critical micelle concentration (CMC) values. GML was more potent than LA on account of a lower CMC value, which could be explained by the tendency of nonionic compounds to aggregate more favorably than otherwise structurally similar anionic compounds.[14] Furthermore, it was shown that another fatty acid and monoglyceride pair, capric acid (C10:0) and monocaprin, exhibits similar trends in the type and CMC-dependence of membrane morphological changes.[25]

To date, all SLB studies involving fatty acids and monoglycerides have been conducted in near-neutral pH conditions, and there is an outstanding need to further characterize their membrane-disruptive activities in more diverse, biologically relevant conditions. For example, fatty acids and monoglycerides are biologically active on the skin surface, which is an acidic environment and pH 4.7 is the optimal value for healthy skin.[26] Exogenous addition of these compounds also represents a potential therapeutic strategy for topical skin applications.[27−29] Considering that the acid dissociation constant of fatty acids lies in the acidic regime, it is important to characterize the interaction of LA with phospholipid membranes in acidic pH conditions. Indeed, LA possesses an ionizable carboxylic acid functional group and can exist in neutral or anionic states depending on the pH condition (Figure 1). GML is another promising antimicrobial

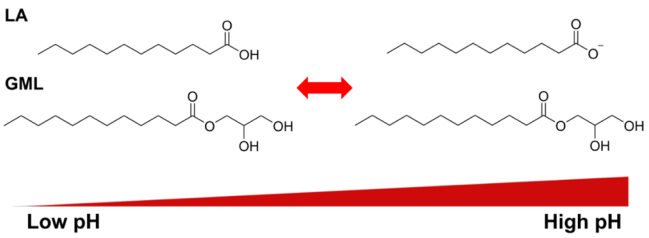

Figure 1. Molecular structures of LA and GML under low (4.5, acidic) and high (7.4, near-neutral) pH conditions. LA has an ionizable carboxylic acid group that undergoes protonation/deprotonation depending on the pH condition. By contrast, GML is nonionic.

lipid that warrants further investigation because of its high potency. In contrast to LA, GML does not possess an ionizable functional group and understanding how the solution pH affects its membrane-disruptive activity would also provide insight into how pH-dependent lipid bilayer properties might affect resulting membrane morphological changes.

To address these outstanding questions, the objective of this study was to investigate how LA and GML interact with SLBs under acidic pH conditions. Multiple biophysical measurement techniques were applied to characterize membrane-disruptive activities, and comparative measurements were made in near-neutral pH conditions. The results enabled us to determine how acidic pH conditions influence membrane-disruptive activities, including characterizing the potency and types of membrane morphological changes that are caused by LA and GML along with their corresponding micellar aggregation properties. Taken together, this integrated experimental approach allowed us to generate mechanistic insights into how solution pH influences the membrane-disruptive activities of LA and GML.

MATERIALS AND METHODS

Materials. Phospholipids for SLB fabrication were obtained as-supplied in chloroform from Avanti Polar Lipids, Inc. (Alabaster, AL). LA and GML were acquired from Sigma-Aldrich (St. Louis, MO) and Abcam (Cambridge, UK), respectively. Phosphate-buffered saline (PBS) was purchased from Gibco (Carlsbad, CA). All solutions were prepared with Milli-Q-treated deionized water (>18 MΩ·cm resistivity) (MilliporeSigma, Billerica, MA).

Preparation of Lipid Solutions. Stock solutions of LA and GML dissolved in ethanol were prepared by weighing the appropriate amount of lyophilized compound and dissolving in ethanol to a concentration of 400 or 200 mM, respectively. Before the experiment, aliquots were diluted 100-fold with a PBS buffer solution to the highest test concentration of 4 and 2 mM for LA and GML, respectively. To promote solubilization, the samples were heated to 70 °C for 30 min and then cooled down before measurements were conducted at room temperature.

Fluorescence Spectroscopy. The CMC values of LA and GML in the appropriate pH conditions were determined by fluorescence spectroscopy measurements, which were conducted using a Cary Eclipse fluorescence spectrophotometer (Varian Inc., Australia). Specifically, 1-pyrenecarboxaldehyde was employed as a fluorescent probe that is sensitive to the presence of micellar aggregates. The test samples were prepared by adding a small aliquot of the fluorescent probe (5 mM) in methanol to a glass tube, and then the methanol was evaporated to form a dry thin film of the probe compound on the glass walls. Afterward, the designated concentration of LA or GML in the appropriate solution was added to the vial, and the sample was vortexed followed by heating to 70 °C. Finally, the sample was cooled down before measurements were conducted at room temperature. The final concentration of the probe was 0.1 μM. In the measurements, the test samples were excited at 365.5 nm, and the emission spectrum was recorded from 400 to 600 nm. The highest-intensity wavelength in the emission spectrum was recorded for each measurement, and the mean and standard deviation are reported from six technical replicates.

Quartz Crystal Microbalance-Dissipation. Quartz crystal microbalance-dissipation (QCM-D) experiments were performed to characterize SLB formation and to detect membrane morphological responses that occurred when test compounds (LA or GML) were added to the SLB platforms. The measurements were conducted with a four-channel Q-Sense E4 instrument (Biolin Scientific AB, Stockholm, Sweden), with simultaneous time-lapsed recording of shifts in the resonance frequency (Δf) and energy dissipation (ΔD) of an oscillating, piezoelectric quartz crystal.[30] The sensor chips had a fundamental frequency of 5 MHz and were coated with a sputter-coated, 50 nm thick layer of silicon dioxide (model no. QSX 303, Biolin Scientific). Before the experiment, the chips were sequentially rinsed with water and ethanol, dried with a stream of nitrogen gas, and treated with oxygen plasma for 1 min using an Expanded Plasma Cleaner (model no. PDC-002, Harrick Plasma, Ithaca, NY). After cleaning, the chips were immediately loaded into the measurement chambers and buffer solution was injected to establish a measurement baseline. All samples were injected at a flow rate of 50 μL/min, as controlled by a peristaltic pump (Reglo Digital, Ismatec, Glattbrugg, Switzerland). The temperature in the measurement chamber was

DOI: 10.1021/acs.langmuir.8b02536
Langmuir 2018, 34, 13745−13753

maintained at 25.0 ± 0.5 °C. The measurement data were recorded at the third (n = 3), fifth (n = 5), and seventh (n = 7) odd overtones using the QSoft software program (Biolin Scientific AB), and the data were normalized according to the overtone number. Data processing was performed in the QTools (Biolin Scientific AB) and OriginPro 8.5 (OriginLab, Northampton, MA) software programs. All presented data were collected at the fifth overtone.

Fluorescence Microscopy. Epifluorescence microscopy experiments were conducted to directly observe morphological changes in the SLBs on glass surfaces upon treatment with LA or GML. The experiments were conducted using an Eclipse Ti-E inverted microscope (Nikon, Tokyo, Japan) with a 60× magnification (NA = 1.49) oil-immersion objective lens (Nikon), and images were collected with an iXon3 512 pixel × 512 pixel EMCCD camera (Andor Technology, Belfast, Northern Ireland). The pixel size was 0.267 × 0.267 μm^2. A fiber-coupled mercury lamp (Intenslight C-HGFIE, Nikon) was used to illuminate fluorescently labeled phospholipids (0.5 mol % rhodamine-DHPE) with a TRITC filter. For the experiments, SLBs were formed on a glass slide that was enclosed within a microfluidic flow-through chamber (sticky slide VI 0.4, Ibidi, Germany), and the solvent-assisted lipid bilayer (SALB) method was employed as reported elsewhere.[31,32] After SLB formation, the measurement chamber was rinsed with PBS buffer solution, and then the test compound was added under continuous flow conditions at a flow rate of 50 μL/min. Time-lapse micrographs were recorded every 5 s for a total duration of 30 min, and the initial time, t = 0 s, was defined by when the test compound solution was injected.

RESULTS AND DISCUSSION

Effect of Solution pH on CMC. To determine how solution pH affects the CMC values of LA and GML, we conducted fluorescence spectroscopy experiments based on detecting the partitioning of a fluorescent molecule, 1-pyrenecarboxaldehyde, into micellar aggregates (Figure 2). In aqueous environments, 1-pyrenecarboxaldehyde has a peak emission wavelength of around 473 nm, and the peak wavelength decreases in the presence of micellar aggregates as the dielectric constant of the surrounding environment

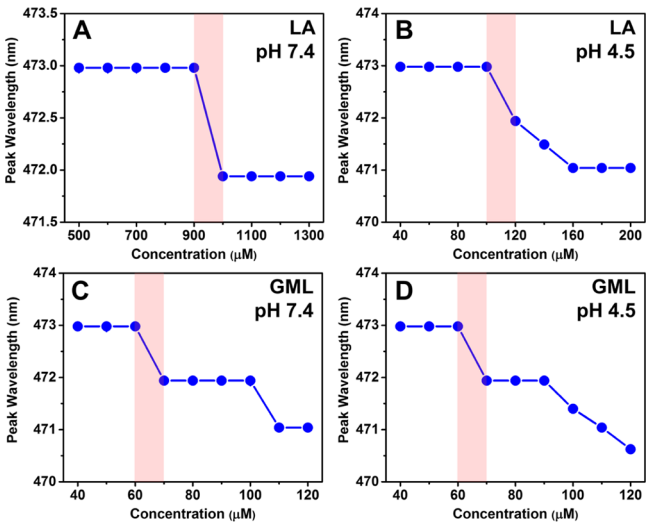

Figure 2. Determination of CMC for LA and GML in different pH environments. Peak wavelength is shown as a function of compound concentration in the PBS solution for (A) LA at pH 7.4, (B) LA at pH 4.5, (C) GML at pH 7.4, and (D) GML at pH 4.5. Each point in the graph represents the average value of the six scans (n = 6). The CMC value is defined as the highest test concentration before the first break point occurs.

becomes lower.[33] Hence, the CMC value of a test compound in particular aqueous conditions can be readily assessed by incubating different concentrations of the compound with the fluorescent probe and defining the CMC as the lowest concentration at which the peak wavelength begins to decrease relative to the baseline value. The CMC experiments were conducted under pH 7.4 and 4.5 conditions that encompass typical values for physiological (blood) and skin pH levels, respectively.

We first measured the CMC value of LA under pH 7.4 conditions and determined a CMC value of 900 μM, which agrees well with the previous literature values that were obtained in similar ionic strength and pH conditions[34] (Figure 2A). By contrast, under pH 4.5 conditions, the CMC value of LA decreased to 100 μM, demonstrating that micellar aggregation of LA is more thermodynamically favorable under acidic pH conditions (Figure 2B). This trend is consistent with the ionization properties of LA as it is known that the pK_a value of LA is ∼5 (refs[35,36]). In our particular system, it was determined that the pK_a value of LA is 5.8 (Figure S1). Hence, at pH 7.4, the carboxylic acid groups on nearly all LA molecules (98%) are deprotonated and there is significant charge repulsion between the anionic LA molecules.[37] On the other hand, at pH 4.5, 95% of the LA molecules are protonated and there is less repulsion, which is consistent with a lower CMC value.

In addition, the CMC value of GML was measured in pH 7.4 and 4.5 conditions and was found to be 60 μM in both cases (Figure 2C,D). This finding is consistent with GML's molecular properties as a nonionic compound that is formed by the esterification of LA and glycerol, and it is not ionizable across the tested pH range. Taken together, the experimental results demonstrate that the micellar aggregation properties of LA and GML exhibit differing sensitivities to the solution pH, and these differences can be rationalized by taking into account the molecular properties of the two compounds. It is particularly noteworthy that the CMC value of LA shifts down to 100 μM at pH 4.5, suggesting that it may have more potent membrane-disruptive activities under acidic conditions.

Effect of Compound Treatment on SLBs. QCM-D experiments were conducted to measure the concentration-dependent activities of LA and GML acting against SLBs under pH 7.4 (near-neutral) and 4.5 (acidic) conditions. In QCM-D measurements, changes in resonance frequency (Δf) and energy dissipation (ΔD) of an oscillating quartz crystal sensor chip are tracked as a function of time and correlate with the acoustic mass (biomolecular mass and hydrodynamically coupled solvent mass) and viscoelastic properties of an adsorbed thin film on the sensor surface, respectively. A negative Δf shift corresponds to an increase in the acoustic mass whereas a positive ΔD shift relates to an increase in the film viscoelasticity. SLBs composed of 1,2-dioleoyl-*sn*-glycero-3-phosphocholine (DOPC) phospholipid were fabricated at the appropriate pH condition on silicon dioxide-coated sensor surfaces by the SALB method[31,38] and provided the measurement platform on which membrane morphological responses were detected. Specifically, the reported baseline measurement values correspond to intact SLB platforms and then LA or GML in an equivalent buffer solution was added to the measurement chamber under continuous flow conditions starting at t = 5 min. The resulting Δf and ΔD signals occurred due to membrane morphological changes and the specific type of morphological response was assigned based on

DOI: 10.1021/acs.langmuir.8b02536
Langmuir 2018, 34, 13745−13753

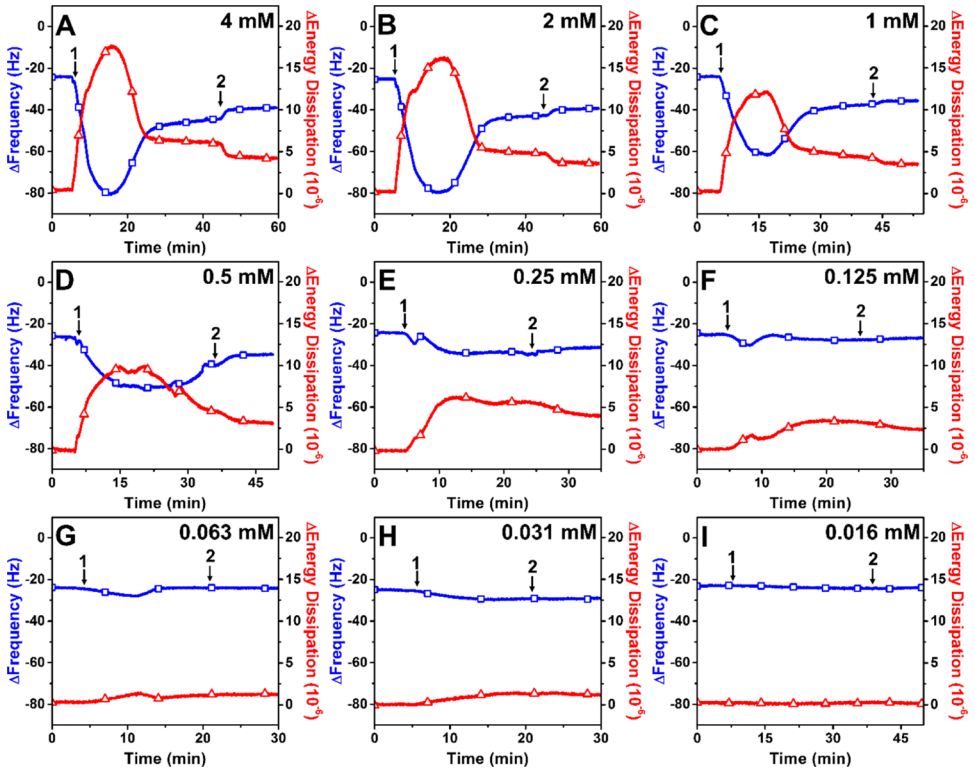

Figure 3. QCM-D investigation of LA treatment on SLBs at pH 4.5. Δf (blue line with squares) and ΔD (red line with triangles) shifts are presented as a function of time for (A) 4 mM, (B) 2 mM, (C) 1 mM, (D) 500 μM, (E) 250 μM, (F) 125 μM, (G) 63 μM, (H) 31 μM, and (I) 16 μM LA. The baseline values at t = 0 min correspond to an SLB platform on the sensor surface. LA was added at t = 5 min (arrow 1), and a buffer washing step was performed (arrow 2) after the measurement signals stabilized.

the previous works.[14,25] After the measurement response stabilized, a washing step with an equivalent buffer solution was performed. The results obtained for LA and GML are presented below.

Lauric Acid. LA addition to SLBs under the pH 7.4 condition followed established trends showing concentration-dependent tubule formation at 1 mM and higher LA concentrations (Figure S2). Specifically, two-step interaction kinetics were observed. By contrast, at 500 μM LA, the measurement responses were negligible, indicating no interaction in this low concentration regime. These data are consistent with LA being active only at and above its CMC value, which was 900 μM as determined in this study (cf. Figure 2A).

In marked contrast, LA addition to SLBs under the pH 4.5 condition induced appreciably larger changes in the Δf and ΔD signals that reached around −85 Hz and 17 × 10^{-6}, respectively, for 4 mM LA (Figure 3A). A subsequent buffer washing step had minor effect on the measurement responses. Similar results were obtained for 2 mM LA, and concentration-dependent responses with matching kinetic profiles were observed down to 500 μM LA (Figure 3B−D). The magnitude of the measurement responses, particularly the large ΔD shifts, supports that the resulting membrane morphological responses arise from budding-like behavior rather than tubule formation. In the range of 250−125 μM LA, the Δf shifts were appreciably smaller whereas significant ΔD shifts were observed around 2−5 × 10^{-6} (Figure 3E,F). These responses suggest a reordering of the membrane components, as commonly found for membranes in different phase states.[39] At lower LA concentrations, the measurement responses were nearly negligible (Figure 3G−I). Together, these data support that LA induces distinct membrane morphological responses under the pH 4.5 condition, which resemble membrane budding during the initial interaction stage. This pattern is also consistent with the fact that most LA molecules are protonated at pH 4.5, and therefore behave more like neutral compounds (e.g., monoglycerides) with greater rates of membrane translocation, hence altering the membrane strain profile. Another important finding is that LA was active down to 125 μM under the pH 4.5 condition, and this is also consistent with its corresponding CMC value of 100 μM as measured in this study (cf. Figure 2B). Hence, the data support that LA is more potent against lipid bilayers under acidic conditions, as determined by the lower minimum concentration at which it induces membrane morphological responses.

Glycerol Monolaurate. GML addition to SLBs under the pH 7.4 condition revealed a combination of membrane budding and membrane-lytic behavior, as evidenced by particularly disruptive activity at 1 mM and higher GML concentrations and more prominent membrane budding in the range of 500−125 μM GML (Figure S3). The GML concentration-dependent membrane budding responses were also observed at 63 GML, whereas nearly negligible activity was observed at 31 μM and lower GML concentrations. Taken together, the observed trends support that membrane budding is the predominant membrane morphological response observed upon GML treatment, and the range of the active GML concentrations is consistent with the CMC value measured in this study (cf. Figure 2C).

Under the pH 4.5 condition, GML addition also caused membrane budding, although the extent of the QCM-D

DOI: 10.1021/acs.langmuir.8b02536
Langmuir 2018, 34, 13745−13753

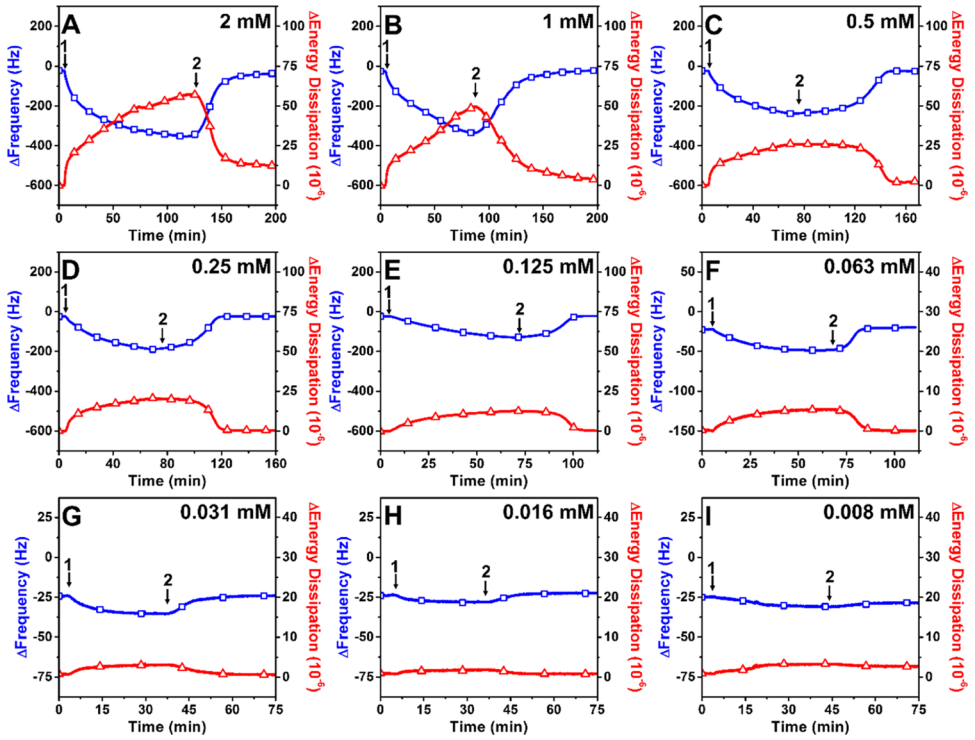

Figure 4. QCM-D investigation of GML treatment on SLBs at pH 4.5. Δf (blue line with squares) and ΔD (red line with triangles) shifts are presented as a function of time for (A) 2 mM, (B) 1 mM, (C) 500 μM, (D) 250 μM, (E) 125 μM, (F) 63 μM, (G) 31 μM, (H) 16 μM, and (I) 8 μM GML. The baseline values at t = 0 min correspond to an SLB platform on the sensor surface. GML was added at t = 5 min (arrow 1), and a buffer washing step was performed (arrow 2) after the measurement signals stabilized.

measurement responses was significantly larger than that under the pH 7.4 condition (Figure 4). At 2 mM GML, the Δf shift decreased to around −340 Hz and the corresponding ΔD shift was around 55 × 10^{-6}, with both responses reaching nearly stable values (Figure 4A). On buffer washing, the Δf shift returned to nearly baseline values whereas the ΔD shift stabilized around 13 × 10^{-6}. Similar measurement responses were observed in a GML concentration-dependent fashion down to around 31 μM GML (Figure 4B−G). The magnitudes of the Δf and ΔD responses in this concentration regime were comparable to those obtained under the pH 7.4 condition. Furthermore, 16 μM and lower GML concentrations were inactive against SLBs under the pH 4.5 condition, demonstrating that GML activity against the SLBs followed a similar concentration-dependent trend across the two tested pH conditions (Figure 4H,I). The results also agree with the measured CMC value of GML at pH 4.5 (cf. Figure 2D).

Compared to the pH 7.4 condition, two significant differences were observed when GML was added to the SLBs under the pH 4.5 condition. First, more pronounced lytic activity was observed under the pH 7.4 condition, whereas a greater extent of membrane budding occurred under the pH 4.5 condition. This difference likely relates to the fact that the bending stiffness of the phosphatidylcholine bilayers can decrease under acidic conditions[40,41] and therefore accommodate more strain before the onset of membrane lysis. Second, the larger QCM-D measurement responses indicated that there was more significant membrane remodeling in response to GML-induced membrane strain under the pH 4.5 condition. This latter observation is also likely related to the decrease in membrane bending stiffness which facilitates greater responsiveness to the applied strain.

Observation of Membrane Morphological Changes. To complement the QCM-D measurements, time-lapsed epifluorescence microscopy experiments were conducted to enable direct observation of membrane morphological changes in the SLBs. The SLBs were composed of 99.5 mol % DOPC and 0.5 mol % 1,2-dipalmitoyl-*sn*-glycero-3-phosphoethanolamine-*N*-(lissamine rhodamine B sulfonyl)phospholipid and prepared via the SALB method on a hydrophilic glass surface that was enclosed within a microfluidic chamber to control the introduction of liquid sample. The SLB was formed at the appropriate pH condition (7.4 or 4.5, depending on the experiment), and once a baseline signal was established, either LA or GML in an equivalent buffer solution was added under continuous flow conditions. The time point labeled "t = 0 min" indicates when the solution containing the test compound (LA or GML) reached the measurement chamber. On the basis of the fluorescence spectroscopy and QCM-D measurement results, we tested LA treatment at 2 mM and 250 μM concentrations. At the former concentration, the LA molecules are in the micellar state at both the tested pH conditions, whereas at the latter concentration, the LA molecules are in the micellar state only under the acidic condition. We also tested 500 μM GML treatment at both pH conditions to understand how solution pH affects the extent of GML-induced membrane remodeling.

2 mM LA. Figure 5A presents time-lapsed snapshots of membrane morphological responses that occur when 2 mM LA is added to an SLB platform under the pH 7.4 condition (see also Video S1). Within a few minutes, elongated tubules began to protrude from the SLB and became aligned with the flow direction in the microfluidic chamber. After rinsing was performed, the tubules were removed and the underlying SLB

DOI: 10.1021/acs.langmuir.8b02536
Langmuir 2018, 34, 13745−13753

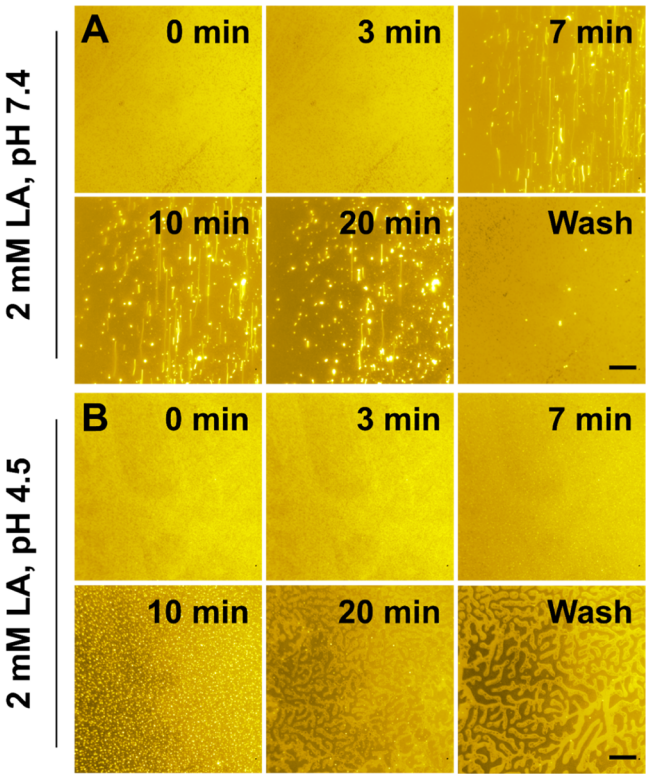

Figure 5. Microscopic observation of 2 mM LA-induced membrane morphological responses on SLBs. (A) Image snapshots at various time points depict nucleation sites from which tubules grow upon LA treatment of SLB at pH 7.4. (B) Image snapshots at various time points depict nucleation sites from which buds grow and membrane phase separation occurs upon LA treatment of SLB at pH 4.5. t = 0 min corresponds to the introduction of 2 mM LA solution into the measurement chamber. The scale bar is 20 μm.

appeared to be largely intact. Overall, the observed results agree well with our previous report[14] and provide control data to compare with membrane morphological responses observed under acidic conditions.

In marked contrast, Figure 5B shows that when 2 mM LA was added to an SLB platform under the pH 4.5 condition, small buds formed within 10 min and are reminiscent of the membrane morphological responses that occur upon treatment with monocaprin[25]—a monoglyceride of similar molecular length (see also Video S2). However, protonated LA molecules induced particular membrane morphological changes that are quite distinct from treatment with monoglycerides. Over time, the number of buds decreased while fluorescent microstructures appeared in the SLB, giving rise to an archipelago effect that was characterized by darker regions with lower fluorophore concentrations and brighter regions with higher fluorophore concentrations.[42] These features are consistent with phase separation of two coexisting phases with a low line tension, as previously reported for SLBs with high cholesterol fractions.[42,43] Upon buffer washing, the two coexisting phases remained evident and hence, LA treatment appeared to induce phase separation in the SLB. The observed behaviors are very different from the LA treatment at pH 7.4, where tubule formation occurred without phase separation. As such, the principal effect of LA treatment at pH 4.5 is inducing membrane phase separation in the SLB, which is distinct from its role in promoting tubule formation at pH 7.4.

250 μM LA. The effect of 250 μM LA treatment was also tested to observe the membrane morphological responses in a condition where LA is in the micellar state only under acidic conditions. Indeed, Figure 6A shows that 250 μM LA

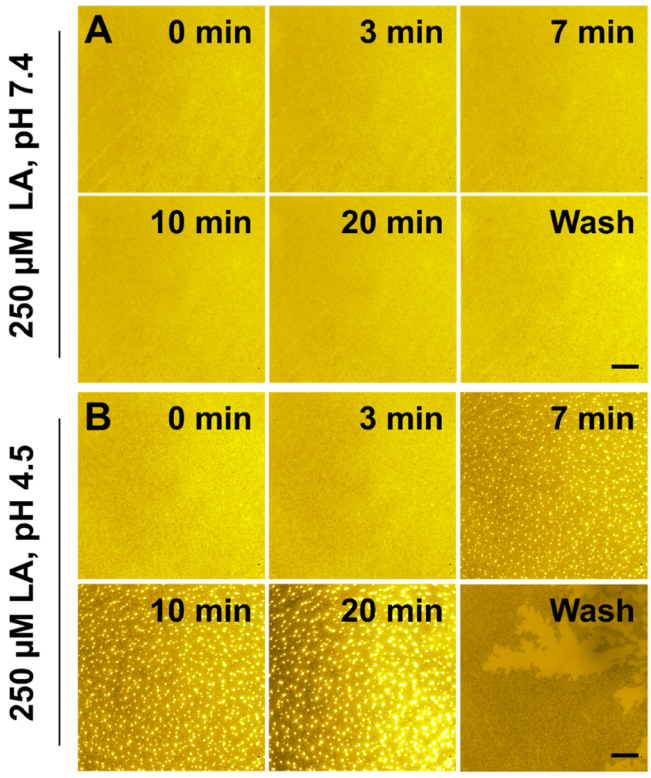

Figure 6. Microscopic observation of 250 μM LA-induced membrane morphological responses on SLBs. (A) Image snapshots at various time points depict the lack of membrane morphological response upon LA treatment of SLB at pH 7.4. (B) Image snapshots at various time points depict nucleation sites from which buds grow and membrane phase separation occurs upon LA treatment of SLB at pH 4.5. t = 0 min corresponds to the introduction of 250 μM LA solution into the measurement chamber. The scale bar is 20 μm.

treatment has negligible effect on the SLB under the pH 7.4 condition, and this lack of activity is consistent with the monomeric state of the LA molecules in this condition. By contrast, as presented in Figure 6B, 250 μM LA treatment of the SLB platform under the pH 4.5 condition induced membrane budding within a few minutes (see also Video S3). The buds remained stable, and extensive phase separation was not observed during the treatment step. Upon buffer washing, there was also evidence of membrane phase separation, although striping was not prominent. Together, these results support that LA is more potent against SLBs under acidic conditions, and the observed trends agree well with the measured CMC values. Hence, LA in acidic conditions initially induces membrane budding leading to membrane phase separation and is active at lower bulk concentrations. By contrast, LA in neutral pH conditions causes tubule formation and is only active at appreciably higher bulk concentrations.

500 μM GML. We also investigated the effect of 500 μM GML treatment on SLBs under both the tested pH conditions. As shown in Figure 7A, GML treatment under the pH 7.4 condition induced membrane budding. The time-lapsed

DOI: 10.1021/acs.langmuir.8b02536
Langmuir 2018, 34, 13745−13753

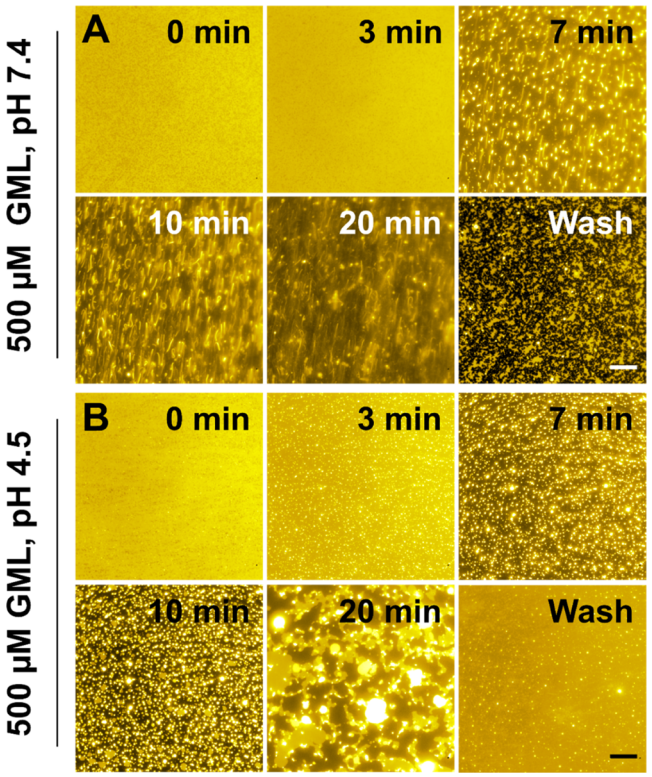

Figure 7. Microscopic observation of 500 μM GML-induced membrane morphological responses on SLBs. (A) Image snapshots at various time points depict nucleation sites from which entangled tubes form, causing membrane budding and membrane lysis, upon GML treatment of SLB at pH 7.4. (B) Image snapshots at various time points depict nucleation sites from which buds grow upon GML treatment of SLB at pH 4.5. t = 0 min corresponds to the introduction of 500 μM GML solution into the measurement chamber. The scale bar is 20 μm.

micrographs indicate that some tubules formed initially and became entangled, giving rise to the buds. These observations agree well with past results,[14] while it was further seen that, upon buffer washing, GML treatment caused some degree of membrane lysis (see also Video S4). On the other hand, Figure 7B shows that the GML treatment at pH 4.5 induced more extensive membrane budding, and the buds coalesced to form larger bud-like structures, likely as a means of relieving membrane tension (see also Video S5). Compared to the pH 7.4 condition, the buds were appreciably larger in the pH 4.5 condition. This result is consistent with the QCM-D results and likely reflects the lower membrane bending stiffness, which facilitates more extensive membrane remodeling. On buffer washing, the large bud structures were removed, while the underlying bilayer remained intact with nearly uniform fluorescence intensity.

Some bright spots appeared on the bilayer surface and likely correspond to the nucleation sites, whereas the extent of membrane lysis was negligible in the pH 4.5 condition as compared to the pH 7.4 condition. As such, GML treatment induced the formation of entangled tubules and/or buds in both cases, although the extent of membrane remodeling strongly depended on the solution pH. The observed trend agrees well with the QCM-D measurement results and indicates that the extent of possible membrane remodeling is greater at pH 4.5, whereas the concentration-dependent activity trend of GML is equivalent across the tested pH conditions.

CONCLUSIONS

In this work, we have employed SLB platforms to understand how LA and GML interact with lipid bilayers under acidic pH conditions and compared the results with those obtained in near-neutral pH conditions. Two pH conditions were selected for testing, pH 4.5 and 7.4, which correspond to skin-like and physiological (blood) environments, respectively. While the CMC of LA was 900 μM at pH 7.4, it decreased to 100 μM at pH 4.5, and this finding is consistent with the pK_a value of LA, which was determined to be around 5.8. Specifically, the decrease in CMC occurs because the majority of LA molecules are protonated under acidic conditions, and hence, micellar aggregation becomes more thermodynamically favorable. On the other hand, the CMC of GML was 60 μM in both cases, and the observed lack of pH dependence in its micellar aggregation properties is consistent with its nonionic character. Using the QCM-D and time-lapsed fluorescence microscopy techniques, we discovered that LA causes membrane phase separation in lipid bilayers under the pH 4.5 condition. This membrane interaction was strikingly different from the tubule formation that is observed when LA interacts with lipid bilayers at pH 7.4. The trend in minimum concentrations of LA that was required for membrane-disruptive activity in the SLB platform was also in excellent agreement with the measured CMC values. Likewise, GML induced membrane budding in both the tested pH conditions, with a similar GML concentration-dependent profile that fits well with its pH-stable CMC value. Of note, the extent of GML-induced membrane budding varied depending on the pH condition, offering insight into how the pH-dependent mechanical properties of lipid bilayers also influence the membrane remodeling process. As such, solution pH had a dramatic influence on how LA interacts with lipid bilayers via causing tubule formation or membrane phase separation, and it also affected the extent of membrane remodeling in response to the GML treatment. In summary, the findings demonstrate how solution pH can have a dramatic effect on the membrane-disruptive behaviors of LA and GML and motivate further exploration of these activities in biological contexts.

ASSOCIATED CONTENT

Supporting Information

The Supporting Information is available free of charge on the ACS Publications website at DOI: 10.1021/acs.langmuir.8b02536.

Descriptions of pK_a determination for LA and QCM-D measurements for concentration-dependent interactions of LA and GML with SLBs at pH 7.4 (PDF)

Microscopic observation of 2 mM LA-induced tubule formation on an SLB at pH 7.4 (AVI)

Microscopic observation of 2 mM LA-induced budding and membrane phase separation on an SLB at pH 4.5 (AVI)

Microscopic observation of 250 μM LA-induced budding and membrane phase separation on an SLB at pH 4.5 (AVI)

Microscopic observation of 500 μM GML-induced membrane budding and lysis on an SLB at pH 7.4 (AVI)

DOI: 10.1021/acs.langmuir.8b02536
Langmuir 2018, 34, 13745−13753

Microscopic observation of 500 μM GML-induced spherical protrusions on an SLB at pH 4.5 (AVI)

AUTHOR INFORMATION

Corresponding Author

*E-mail: njcho@ntu.edu.sg.

ORCID

Joshua A. Jackman: 0000-0002-1800-8102

Nam-Joon Cho: 0000-0002-8692-8955

Notes

The authors declare no competing financial interest.

ACKNOWLEDGMENTS

This work was supported by a National Research Foundation Proof-of-Concept Grant (NRF2015NRF-POC001-019), an A*STAR-NTU-NHG Skin Research Grant (SRG/14028), and the Creative Materials Discovery Program through the National Research Foundation of Korea (NRF) that is funded by the Ministry of Science, ICT, and Future Planning (2016M3D1A1024098). Additional support was provided through the NTU-California Center on Precision Biology.

REFERENCES

(1) Mukai, M.; Regen, S. L. Lipid Raft Formation Driven by Push and Pull Forces. *Bull. Chem. Soc. Jpn.* **2017**, *90*, 1083−1087.

(2) Denisov, I. G.; Sligar, S. G. Nanodiscs in Membrane Biochemistry and Biophysics. *Chem. Rev.* **2017**, *117*, 4669−4713.

(3) Komiyama, M.; Yoshimoto, K.; Sisido, M.; Ariga, K. Chemistry Can Make Strict and Fuzzy Controls for Bio-Systems: DNA Nanoarchitectonics and Cell-Macromolecular Nanoarchitectonics. *Bull. Chem. Soc. Jpn.* **2017**, *90*, 967−1004.

(4) Kroll, A. V.; Fang, R. H.; Zhang, L. Biointerfacing and Applications of Cell Membrane-Coated Nanoparticles. *Bioconjugate Chem.* **2016**, *28*, 23−32.

(5) Thormar, H.; Hilmarsson, H. The Role of Microbicidal Lipids in Host Defense against Pathogens and their Potential as Therapeutic Agents. *Chem. Phys. Lipids* **2007**, *150*, 1−11.

(6) Yoon, B.; Jackman, J.; Valle-González, E.; Cho, N.-J. Antibacterial Free Fatty Acids and Monoglycerides: Biological Activities, Experimental Testing, and Therapeutic Applications. *Int. J. Mol. Sci.* **2018**, *19*, 1114.

(7) Desbois, A. P.; Smith, V. J. Antibacterial Free Fatty Acids: Activities, Mechanisms of Action and Biotechnological Potential. *Appl. Microbiol. Biotechnol.* **2010**, *85*, 1629−1642.

(8) Thormar, H. *Lipids and Essential Oils as Antimicrobial Agents*; John Wiley & Sons, 2011.

(9) Drake, D. R.; Brogden, K. A.; Dawson, D. V.; Wertz, P. W. Thematic Review Series: Skin Lipids. Antimicrobial Lipids at the Skin Surface. *J. Lipid Res.* **2008**, *49*, 4−11.

(10) Fischer, C. L.; Blanchette, D. R.; Brogden, K. A.; Dawson, D. V.; Drake, D. R.; Hill, J. R.; Wertz, P. W. The Roles of Cutaneous Lipids in Host Defense. *Biochim. Biophys. Acta, Mol. Cell Biol.* **2014**, *1841*, 319−322.

(11) Chen, Y. E.; Tsao, H. The Skin Microbiome: Current Perspectives and Future Challenges. *J. Am. Acad. Dermatol.* **2013**, *69*, 143−155.

(12) Bergsson, G.; Steingrímsson, Ó.; Thormar, H. Bactericidal Effects of Fatty Acids and Monoglycerides on *Helicobacter pylori*. *Int. J. Antimicrob. Agents* **2002**, *20*, 258−262.

(13) Kabara, J. J.; Swieczkowski, D. M.; Conley, A. J.; Truant, J. P. Fatty Acids and Derivatives as Antimicrobial Agents. *Antimicrob. Agents Chemother.* **1972**, *2*, 23−28.

(14) Yoon, B. K.; Jackman, J. A.; Kim, M. C.; Cho, N.-J. Spectrum of Membrane Morphological Responses to Antibacterial Fatty Acids and Related Surfactants. *Langmuir* **2015**, *31*, 10223−10232.

(15) Kabara, J. J. Antimicrobial Agents Derived from Fatty Acids. *J. Am. Oil Chem. Soc.* **1984**, *61*, 397−403.

(16) Conley, A. J.; Kabara, J. J. Antimicrobial Action of Esters of Polyhydric Alcohols. *Antimicrob. Agents Chemother.* **1973**, *4*, 501−506.

(17) Bergsson, G.; Arnfinnsson, J.; SteingrÍmsson, Ó.; Thormar, H. Killing of Gram-positive Cocci by Fatty Acids and Monoglycerides. *APMIS* **2001**, *109*, 670−678.

(18) Bergsson, G.; Arnfinnsson, J.; Steingrimsson, O.; Thormar, H. In Vitro Killing of *Candida albicans* by Fatty Acids and Monoglycerides. *Antimicrob. Agents Chemother.* **2001**, *45*, 3209−3212.

(19) Hyldgaard, M.; Sutherland, D. S.; Sundh, M.; Mygind, T.; Meyer, R. L. Antimicrobial Mechanism of Monocaprylate. *Appl. Environ. Microbiol.* **2012**, *78*, 2957−2965.

(20) Royce, L. A.; Liu, P.; Stebbins, M. J.; Hanson, B. C.; Jarboe, L. R. The Damaging Effects of Short Chain Fatty Acids on *Escherichia coli* Membranes. *Appl. Microbiol. Biotechnol.* **2013**, *97*, 8317−8327.

(21) Royce, L. A.; Boggess, E.; Fu, Y.; Liu, P.; Shanks, J. V.; Dickerson, J.; Jarboe, L. R. Transcriptomic Analysis of Carboxylic Acid Challenge in *Escherichia coli*: Beyond Membrane Damage. *PLoS One* **2014**, *9*, e89580.

(22) Thid, D.; Benkoski, J. J.; Svedhem, S.; Kasemo, B.; Gold, J. DHA-Induced Changes of Supported Lipid Membrane Morphology. *Langmuir* **2007**, *23*, 5878−5881.

(23) Heerklotz, H. Interactions of Surfactants with Lipid Membranes. *Q. Rev. Biophys.* **2008**, *41*, 205−264.

(24) Staykova, M.; Arroyo, M.; Rahimi, M.; Stone, H. A. Confined Bilayers Passively Regulate Shape and Stress. *Phys. Rev. Lett.* **2013**, *110*, 028101.

(25) Yoon, B. K.; Jackman, J. A.; Kim, M. C.; Sut, T. N.; Cho, N.-J. Correlating Membrane Morphological Responses with Micellar Aggregation Behavior of Capric Acid and Monocaprin. *Langmuir* **2017**, *33*, 2750−2759.

(26) Lambers, H.; Piessens, S.; Bloem, A.; Pronk, H.; Finkel, P. Natural Skin Surface pH is on Average Below 5, which is Beneficial for its Resident Flora. *Int. J. Cosmet. Sci.* **2006**, *28*, 359−370.

(27) Pornpattananangkul, D.; Fu, V.; Thamphiwatana, S.; Zhang, L.; Chen, M.; Vecchio, J.; Gao, W.; Huang, C. M.; Zhang, L. In Vivo Treatment of *Propionibacterium acnes* Infection with Liposomal Lauric Acids. *Adv. Healthcare Mater.* **2013**, *2*, 1322−1328.

(28) Flanagan, J. L.; Khandekar, N.; Zhu, H.; Watanabe, K.; Markoulli, M.; Flanagan, J. T.; Papas, E. Glycerol Monolaurate Inhibits Lipase Production by Clinical Ocular Isolates Without Affecting Bacterial Cell Viability Glycerol Monolaurate Inhibits Bacterial Lipase Production. *Invest. Ophthalmol. Visual Sci.* **2016**, *57*, 544−550.

(29) Mueller, E. A.; Schlievert, P. M. Non-Aqueous Glycerol Monolaurate Gel Exhibits Antibacterial and Anti-Biofilm Activity against Gram-Positive and Gram-Negative Pathogens. *PLoS One* **2015**, *10*, e0120280.

(30) Rodahl, M.; Höök, F.; Krozer, A.; Brzezinski, P.; Kasemo, B. Quartz Crystal Microbalance Setup for Frequency and Q-Factor Measurements in Gaseous and Liquid Environments. *Rev. Sci. Instrum.* **1995**, *66*, 3924−3930.

(31) Tabaei, S. R.; Choi, J.-H.; Haw Zan, G.; Zhdanov, V. P.; Cho, N.-J. Solvent-Assisted Lipid Bilayer Formation on Silicon Dioxide and Gold. *Langmuir* **2014**, *30*, 10363−10373.

(32) Tabaei, S. R.; Jackman, J. A.; Kim, M.; Yorulmaz, S.; Vafaei, S.; Cho, N.-J. Biomembrane Fabrication by the Solvent-Assisted Lipid Bilayer (SALB) Method. *J. Visualized Exp.* **2015**, *106*. DOI: 10.3791/53073

(33) Ananthapadmanabhan, K.; Goddard, E.; Turro, N.; Kuo, P. Fluorescence Probes for Critical Micelle Concentration. *Langmuir* **1985**, *1*, 352−355.

(34) Kanicky, J. R.; Shah, D. O. Effect of Premicellar Aggregation on the pK_a of Fatty Acid Soap Solutions. *Langmuir* **2003**, *19*, 2034−2038.

(35) Goodman, D. S. The Distribution of Fatty Acids between N-Heptane and Aqueous Phosphate Buffer. *J. Am. Chem. Soc.* **1958**, *80*, 3887−3892.

DOI: 10.1021/acs.langmuir.8b02536
Langmuir 2018, 34, 13745−13753

(36) Spector, A. A. Fatty Acid Binding to Plasma Albumin. *J. Lipid Res.* **1975**, *16*, 165−179.
(37) Small, D. *Physical Properties of Fatty Acids and their Extracellular and Intracellular Distribution*; Nestle Nutrition Workshop Series: USA, 1992.
(38) Tabaei, S. R.; Jackman, J. A.; Kim, S.-O.; Zhdanov, V. P.; Cho, N.-J. Solvent-Assisted Lipid Self-Assembly at Hydrophilic Surfaces: Factors Influencing the Formation of Supported Membranes. *Langmuir* **2015**, *31*, 3125−3134.
(39) Kawakami, L. M.; Yoon, B. K.; Jackman, J. A.; Knoll, W.; Weiss, P. S.; Cho, N.-J. Understanding How Sterols Regulate Membrane Remodeling in Supported Lipid Bilayers. *Langmuir* **2017**, *33*, 14756−14765.
(40) Zhou, Y.; Raphael, R. M. Solution pH Alters Mechanical and Electrical Properties of Phosphatidylcholine Membranes: Relation between Interfacial Electrostatics, Intramembrane Potential, and Bending Elasticity. *Biophys. J.* **2007**, *92*, 2451−2462.
(41) Boggara, M. B.; Faraone, A.; Krishnamoorti, R. Effect of pH and Ibuprofen on the Phospholipid Bilayer Bending Modulus. *J. Phys. Chem. B* **2010**, *114*, 8061−8066.
(42) Tabaei, S. R.; Jackman, J. A.; Liedberg, B.; Parikh, A. N.; Cho, N.-J. Observation of Stripe Superstructure in the β-Two-Phase Coexistence Region of Cholesterol−Phospholipid Mixtures in Supported Membranes. *J. Am. Chem. Soc.* **2014**, *136*, 16962−16965.
(43) Seul, M.; Andelman, D. Domain Shapes and Patterns: the Phenomenology of Modulated Phases. *Science* **1995**, *267*, 476.

DOI: 10.1021/acs.langmuir.8b02536
Langmuir 2018, 34, 13745−13753